RAB1A haploinsufficiency phenocopies the 2p14–p15 microdeletion and is associated with impaired neuronal differentiation

Authors

Jonathan J. Rios, Yang Li, Nandina Paria, ..., Linsley Smith, Carol A. Wise, Mauricio R. Delgado

Correspondence

jonathan.rios@tsrh.org

We identify a dominant *RAB1A*-related neurocognitive disorder with speech and motor delay caused by loss-of-function and dominant-negative mutations in *RAB1A*. We demonstrate an essential role for *RAB1A* in neuronal arborization and implicate *RAB1A* haploinsufficiency in the pathogenesis of neurocognitive manifestations associated with the 2p14–p15 microdeletion syndrome.

Rios et al., 2023, The American Journal of Human Genetics *110*, 2103–2111
December 7, 2023
https://doi.org/10.1016/j.ajhg.2023.10.009

CellPress

RAB1A haploinsufficiency phenocopies the 2p14–p15 microdeletion and is associated with impaired neuronal differentiation

Jonathan J. Rios,[1,2,3,4,*] Yang Li,[1] Nandina Paria,[1] Ryan J. Bohlender,[5] Chad Huff,[5] Jill A. Rosenfeld,[6,7] Pengfei Liu,[6,7] Weimin Bi,[6,7] Kentaro Haga,[8] Mitsunori Fukuda,[8] Shayal Vashisth,[9] Kiran Kaur,[2] Maria H. Chahrour,[2,9,10,11,12] Michael B. Bober,[13,14] Angela L. Duker,[13] Farah A. Ladha,[6] Neil A. Hanchard,[6] Kristhen Atala,[1] Anas M. Khanshour,[1] Linsley Smith,[15] Carol A. Wise,[1,2,3,4] and Mauricio R. Delgado[15,16]

Summary

Hereditary spastic parapareses (HSPs) are clinically heterogeneous motor neuron diseases with variable age of onset and severity. Although variants in dozens of genes are implicated in HSPs, much of the genetic basis for pediatric-onset HSP remains unexplained. Here, we re-analyzed clinical exome-sequencing data from siblings with HSP of unknown genetic etiology and identified an inherited nonsense mutation (c.523C>T [p.Arg175Ter]) in the highly conserved *RAB1A*. The mutation is predicted to produce a truncated protein with an intact RAB GTPase domain but without two C-terminal cysteine residues required for proper subcellular protein localization. Additional *RAB1A* mutations, including two frameshift mutations and a mosaic missense mutation (c.83T>C [p.Leu28Pro]), were identified in three individuals with similar neurodevelopmental presentations. In rescue experiments, production of the full-length, but not the truncated, RAB1a rescued Golgi structure and cell proliferation in *Rab1*-depleted cells. In contrast, the missense-variant RAB1a disrupted Golgi structure despite intact *Rab1* expression, suggesting a dominant-negative function of the mosaic missense mutation. Knock-down of *RAB1A* in cultured human embryonic stem cell-derived neurons resulted in impaired neuronal arborization. Finally, *RAB1A* is located within the 2p14–p15 microdeletion syndrome locus. The similar clinical presentations of individuals with *RAB1A* loss-of-function mutations and the 2p14–p15 microdeletion syndrome implicate loss of *RAB1A* in the pathogenesis of neurodevelopmental manifestations of this microdeletion syndrome. Our study identifies a *RAB1A*-related neurocognitive disorder with speech and motor delay, demonstrates an essential role for RAB1a in neuronal differentiation, and implicates *RAB1A* in the etiology of the neurodevelopmental sequelae associated with the 2p14–p15 microdeletion syndrome.

Hereditary spastic paraparesis (HSP) is a heterogeneous motor neuron disease that often presents with lower extremity weakness and spasticity resulting in an abnormal gait and joint contractures.[1] Due to the vast clinical variability, and because it is often a diagnosis of exclusion, HSP requires genetic confirmation for a definitive diagnosis. The genetic landscape of HSP is complex, and dozens of genes, termed spastic paraplegia (SPG) loci, have been identified.[2,3] While SPG loci are classified as containing variants associated with either dominant or recessive disease, this dichotomy has been challenged by the identification of mutations in *REEP2*[4] (MIM: 609347), *ATL1*[5,6] (SPG3A [MIM: 606439]), *SPAST*[7] (SPG4 [MIM: 604277]), and Paraplegin[8,9] (*SPG7* [MIM: 602783]) implicated in both dominant and recessive disease inheritance. Additionally, a modifier mutation in *SPAST*/SPG4 was associated with differences in disease severity.[10]

Spastic paraparesis is classified as either pure or complicated, with complicated HSP presenting with variable secondary clinical manifestations. Complicated disease more often results from recessive or X-linked mutations, while pure HSP results from dominant or *de novo* mutations.[11] HSP-associated genes, including those associated with pure and complicated forms, encode proteins with functions that converge on pathways critical for proper neuron formation and function.[2,3] The considerable genetic heterogeneity of HSP has prompted clinical evaluation using exome sequencing (ES); however, despite the comprehensive nature of ES, recent studies demonstrated that a majority of individuals with HSP, or other related neurologic conditions, remain without a genetic diagnosis despite

[1]Center for Pediatric Bone Biology and Translational Research, Scottish Rite for Children, Dallas, TX 75219, USA; [2]Eugene McDermott Center for Human Growth and Development, University of Texas Southwestern Medical Center, Dallas, TX 75390, USA; [3]Departments of Pediatrics University of Texas Southwestern Medical Center, Dallas, TX 75390, USA; [4]Department of Orthopaedic Surgery, University of Texas Southwestern Medical Center, Dallas, TX 75390, USA; [5]Department of Epidemiology, MD Anderson Cancer Center, Houston, TX 77030, USA; [6]Department of Molecular & Human Genetics, Baylor College of Medicine, Houston, TX 77030, USA; [7]Baylor Genetics, Houston, TX 77021, USA; [8]Department of Integrative Life Sciences, Graduate School of Life Sciences, Tohoku University, Sendai, Miyagi 980-8578, Japan; [9]Department of Neuroscience, University of Texas Southwestern Medical Center, Dallas, TX 75390, USA; [10]Department of Psychiatry, University of Texas Southwestern Medical Center, Dallas, TX 75390, USA; [11]Peter O'Donnell Brain Institute, University of Texas Southwestern Medical Center, Dallas, TX 75390, USA; [12]Center for the Genetics of Host Defense, University of Texas Southwestern Medical Center, Dallas, TX 75390, USA; [13]Nemours Children's Hospital, Wilmington, DE 19803, USA; [14]Thomas Jefferson University, Philadelphia, PA 19144, USA; [15]Department of Neurology, Scottish Rite for Children, Dallas, TX 75219, USA; [16]Department of Neurology and Neurotherapeutics, University of Texas Southwestern Medical Center, Dallas, TX 75390, USA
*Correspondence: jonathan.rios@tsrh.org
https://doi.org/10.1016/j.ajhg.2023.10.009.

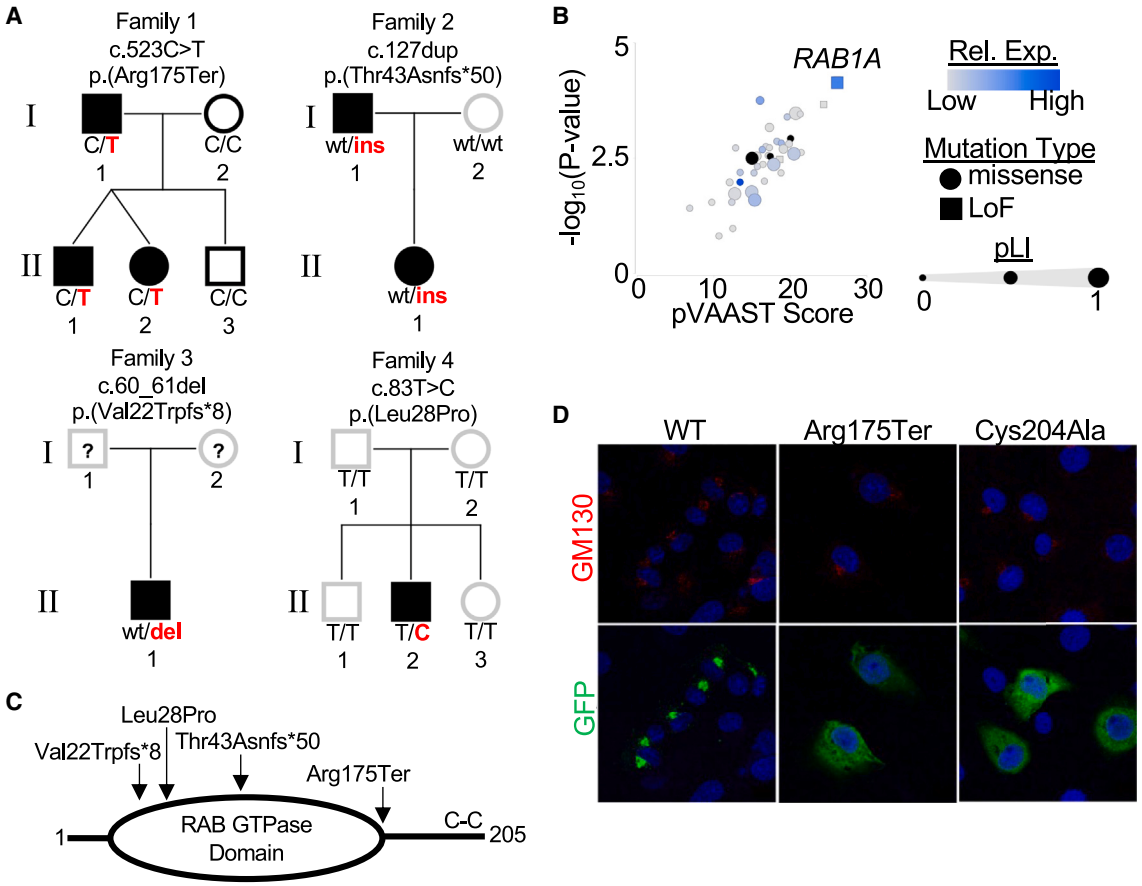

Figure 1. ***RAB1A*** **loss-of-function mutations in families with a dominant developmental and neurocognitive disease**
(A) Pedigrees of families with identified *RAB1A* mutations. Affected individuals are shown with black fill symbols and unaffected with open symbols. Individual *RAB1A* genotypes are shown below. *RAB1A* gene mutations in each pedigree are shown above. Individuals not available for testing and/or lacking clinical evaluations are shown with question mark.
(B) Results of pVAAST analysis for the 44 genes harboring candidate variants in family 1. Genes with loss-of-function (LoF) variants are shown with squares; missense variants are circles. Relative expression of gene orthologs in mouse neurons is shown by blue color. Symbol size reflects the gene pLI score (from gnomAD). Genes without mouse orthologs or without expression data are shown in black.
(C) Schematic showing the GTPase domain and two C-terminal prenylated cysteine residues of RAB1a. Amino acid alterations identified in this study are indicated above.
(D) Representative co-localization of the Golgi-localized GM130 (red) and full-length (WT), truncated (p.Arg175Ter), and cysteine-mutant (p.Cys204Ala) GFP-RAB1a (green) in transfected COS-7 cells.

periodic re-analysis.[12,13] These results suggest that additional disease-causing mutations in other genes remain to be discovered.

We first evaluated a family with paternally inherited complicated HSP (family 1 in Figure 1A). Both siblings presented with neurocognitive differences, developmental motor delay, vision impairment (both siblings wore glasses), and spastic paraplegia (II.1 and II.2 in Figure 1A; Table 1; supplemental note). Brain MRI were normal. The siblings' father was identified with a gait abnormality, lower extremity spasticity, and a past diagnosis of cerebral palsy, although he had a normal birth history and MRI. Clinical ES of both siblings was performed at the Baylor Genetics Laboratory (BGL), as previously described,[14] but this failed to identify genetic diagnoses in either sibling. Following informed consent approved by the Institutional Review Board at the University of Texas Southwestern Medical Center, we performed ES of samples from both parents and integrated results following re-analysis of clinical ES from both siblings. Heterozygous nonsynonymous variants identified in both affected siblings were filtered to include only those with evidence for paternal inheritance, that were not present in an in-house control database, and that were rare (<1% minor allele frequency) in the public Exome Variant Server and ExAC databases. Following filtering, 44 genes harboring candidate variants were prioritized using the gene-based association analysis tool pVAAST (Table S1), which integrates an inheritance LOD score with a deleteriousness score that is then compared to the frequency of similarly deleterious variants in a control population.[15] pVAAST analysis identified nonsense mutations in *RAB1A*, encoding the Ras-related RAB1a, and *CPN1*, encoding the carboxypeptidase N subunit 1, as the most significantly associated genes and with the highest pVAAST scores (Figure 1B; Table S1). The nonsense mutation in *CPN1* was not considered a plausible

Table 1. Clinical characteristics of individuals with *RAB1A* mutations or the 2p14–p15 microdeletion syndrome

Individual	Genotype[a]	Age[b]	Sex	Speech delay	Motor delay	Neurocognition	MRI	Microcephaly	Dysmorphism	Vision	Musculoskeletal	Other	Reference
Family 1, II.1[c]	c.523C>T (p.Arg175Ter)	16 years	male	N/A	yes	learning disability	normal	no	N/A	yes		spastic paraplegia	this report
Family 1, II.2[c]	c.523C>T (p.Arg175Ter)	16 years	female	N/A	yes	sensory integration disorder, dyslexia	normal	no	N/A	yes	bilateral foot cavus, scoliosis	spastic paraplegia	this report
Family 2, II.1	c.127dup (p.Thr43Asnfs*50)	12 years	female	yes	yes	autism, seizures, ID, anxiety	normal	no	yes	light sensitivity	abnormal involuntary movements	hemangioma, constipation, severe insomnia	this report
Family 3, II.1	c.60_61del (p.Val22Trpfs*8)	16 years	male	N/A	N/A	autism, anxiety, aggression	N/A	no	bifid uvula	N/A	hyperextensibility, fatigue, joint pain	tremor, muscle weakness, nephrotic syndrome	this report
Family 4, II.2	c.83T>C (p.Leu28Pro) (mosaic)	15 years	male	yes	yes	abnormal EEG without seizure, cognitive delay, ADHD, anxiety	foreshortened corpus callosum, mildly prominent ventricular system, widening of the foramen of Magendie	yes	yes		spondyloepimetaphyseal dysplasia, scoliosis and spinal fusion, short stature	chronic constipation, periodic limb movement disorder	this report
6	*de novo* 2p14–p15 microdeletion	8 years	male	yes	yes	seizures, ID	normal	yes	yes	hyperopia	N/A		Wohlleber et al.[28]; individual 1
7	*de novo* 2p14–p15 microdeletion	12 years	female	yes	yes	mild ID	normal	yes	yes	no	N/A		Wohlleber et al.[28]; individual 2
8	*de novo* 2p14–p15 microdeletion	4 years	male	yes	yes	N/A	N/A	N/A	yes	yes	hypotonia		Jorgez et al.[26]; individual 2
9	*de novo* 2p14–p15 microdeletion	21 m	male	yes	yes	N/A	cerebral atrophy, colpocephaly, enlarged cisterna magna	yes	yes	N/A	hypotonia	failure to thrive	Jorgez et al.[26]; individual 4
10	*de novo* 2p14–p15 microdeletion	16 years	male	N/A	yes	short attention span, aggression	N/A	yes	yes	N/A	osteopenia, scoliosis, pes planus, ankle eversion	failure to thrive	Jorgez et al.[26]; individual 5
11	*de novo* 2p14–p15 microdeletion	4 years	male	yes	yes	hyperactivity	N/A	N/A	yes	esotropia	mild camptodactyly, pes planus		Jorgez et al.[26]; individual 7
12	*de novo* 2p14–p15 microdeletion	4 years	male	yes	yes	hyperactivity, ID	hemosiderin deposition, changes in lateral ventricles	yes	yes	myopia	delayed tooth eruption	diagnosed spastic cerebral ataxia	Hancarova et al.[27]

N/A, not available or not reported; ID, intellectual disability; EEG, electroencephalogram; ADHD, attention deficit/hyperactivity disorder.
[a]GenBank: NM_004161.5.
[b]Age at publication or genetic testing.
[c]Siblings

candidate because of the low loss-of-function (LoF) intolerance score[16] (gnomAD pLI = 0.00) for *CPN1*, the lack of expression in mouse neurons,[17] and the lack of known involvement in neurologic function and development. Furthermore, mutations in *CPN1* are associated with autosomal-recessive carboxypeptidase N deficiency (MIM: 212070) that is clinically distinct from HSP.

Among all candidate genes with paternally inherited LoF variants, *RAB1A* was the only gene with a LoF intolerance score to suggest selection against haploinsufficiency (gnomAD pLI = 0.82) and was among the most highly expressed orthologous genes in mouse neurons (Figure 1B). Paternal inheritance of the *RAB1A* nonsense mutation (GenBank: NM_004161.5) (c.523C>T [p.Arg175Ter]) was confirmed in both siblings and the affected father by Sanger sequencing; the variant was absent in the mother's and unaffected brother's samples (Figure S1A). To further evaluate the neurodevelopmental abnormalities associated with *RAB1A* haploinsufficiency, we queried the BGL clinical ES database, identifying two additional unrelated individuals with predicted LoF frameshift mutations, each located within the region encoding the RAB GTPase domain (Figure 1A, families 2 and 3). In family 2, the proband (II.1 in Figure 1A) was 3 years of age at the time of testing and is now 12 years of age with a history of speech and motor developmental delay, autism, seizures, facial dysmorphisms, and visual sensitivity to light (family 2, II.1 in Table 1). The father in family 2 was reported to have unspecified developmental delay, learning disability, and abnormal behaviors, though a more detailed clinical evaluation was not available. This frameshift mutation (c.127dup [p.Thr43Asnfs*50]) identified in family 2 was located within exon 3 near the region encoding the N terminus of the protein, suggesting loss of the GTPase domain and premature truncation leading to nonsense-mediated decay (NMD) (Figure 1C). The mutation was confirmed in the proband and father by Sanger sequencing (Figure S1B); the variant was absent in the mother. In family 3, the proband (II.1 in Figure 1A) was 16 years of age at testing, which identified a frameshift mutation (c.60_61del [p.Val22Trpfs*8]) within exon 2 resulting in loss of the GTPase domain, premature truncation, and, likely, NMD (Figures 1A and 1C). Evaluations for speech and motor delay were not available, though he also presented with autism, aggression, bifid uvula (dysmorphism), and muscle weakness (family 3, II.1 in Table 1). Additional genetic analyses in family 3 as well as detailed clinical histories of probands in families 2 and 3 were not available.

Finally, in the course of performing ES in individuals with undiagnosed skeletal dysplasia, we identified a *de novo* mosaic *RAB1A* missense mutation (c.83T>C [p.Leu28Pro]) within the RAB GTPase domain in one proband (Figure 1C; II.2 of family 4 in Figure 1A). Mosaicism was predicted based on the relatively low allele fraction from ES of the individual's blood sample (Table S2), which was confirmed by Sanger sequencing (Figure S1C). To investigate further the potential mosaic nature of this allele, we also sequenced DNA from a saliva sample from the proband. In contrast to results from the blood sample, sequencing of the saliva sample showed equal representation of the heterozygous *RAB1A* alleles, further supporting mosaic differences in the mutant allele burden in this individual. This mosaic individual presented with neurodevelopmental features similar to the others, though he is notable for the more involved skeletal findings (family 4, II.2 in Table 1; supplemental note). Because mutations in *RAB1A* were not previously implicated in a human disease in OMIM, clinical ES of all probands included here failed to identify a genetic diagnosis.

The nonsense mutation identified in family 1 occurs in the last exon of the gene and, therefore, was not predicted to result in nonsense-mediated decay. However, while premature truncation was predicted to maintain a fully intact GTPase domain (Figure 1C), it was also predicted to result in the exclusion of two C-terminal prenylated cysteine residues that direct the subcellular localization and activity of Rab proteins.[18–20] Therefore, we hypothesized that the truncated RAB1a lacking the C-terminal cysteines would mis-localize within cells, resulting in a non-functional protein. A construct encoding an N-terminal GFP-fused RAB1a was transfected into COS-7 cells. Wild-type RAB1a properly co-localized with the Golgi marker GM130 in COS-7 cells, while the truncated RAB1a failed to localize to the Golgi and was detected throughout the cytosol and with no evidence of NMD (Figure 1D). Furthermore, alteration of the two C-terminal cysteine residues to alanine in an otherwise full-length RAB1a was sufficient to cause the same diffuse cellular mis-localization (Figure 1D).

We next tested the function of variant Rab1a in rescue experiments using *Rab1*-cKO cells.[21] *Rab1*-cKO cells were previously engineered from Madin-Darby canine kidney (MDCK) cells to conditionally deplete both endogenous *Rab1a* and *Rab1b*, which have redundant functions in promoting cell survival and proliferation.[22] When *Rab1*-cKO cells are treated with doxycycline and auxin, endogenous Rab1 is depleted, resulting in disruption of Golgi morphology and ER-to-Golgi trafficking.[21] For rescue experiments, constructs encoding wild-type or variant RAB1a were transiently expressed in untreated and treated *Rab1*-cKO cells, followed by evaluation of Golgi morphology and cell proliferation. In untreated *Rab1*-cKO cells, wild-type RAB1a co-localized with AID-tagged Rab1b to the perinuclear Golgi region, while truncated RAB1a remained cytosolic and failed to co-localize with AID-Rab1b (Figure 2A). Golgi morphology was not disrupted following transient expression of constructs encoding full-length or truncated RAB1a (Figure 2A). In treated *Rab1*-depleted cells, full-length RAB1a co-localized with the *trans*-Golgi polypeptide N-acetylgalactosaminyltransferase 2 (GalNT2) and rescued Golgi morphology compared to the empty vector negative control, while the truncated RAB1a did not (Figure 2B). Consistent with these results, production of the full-length

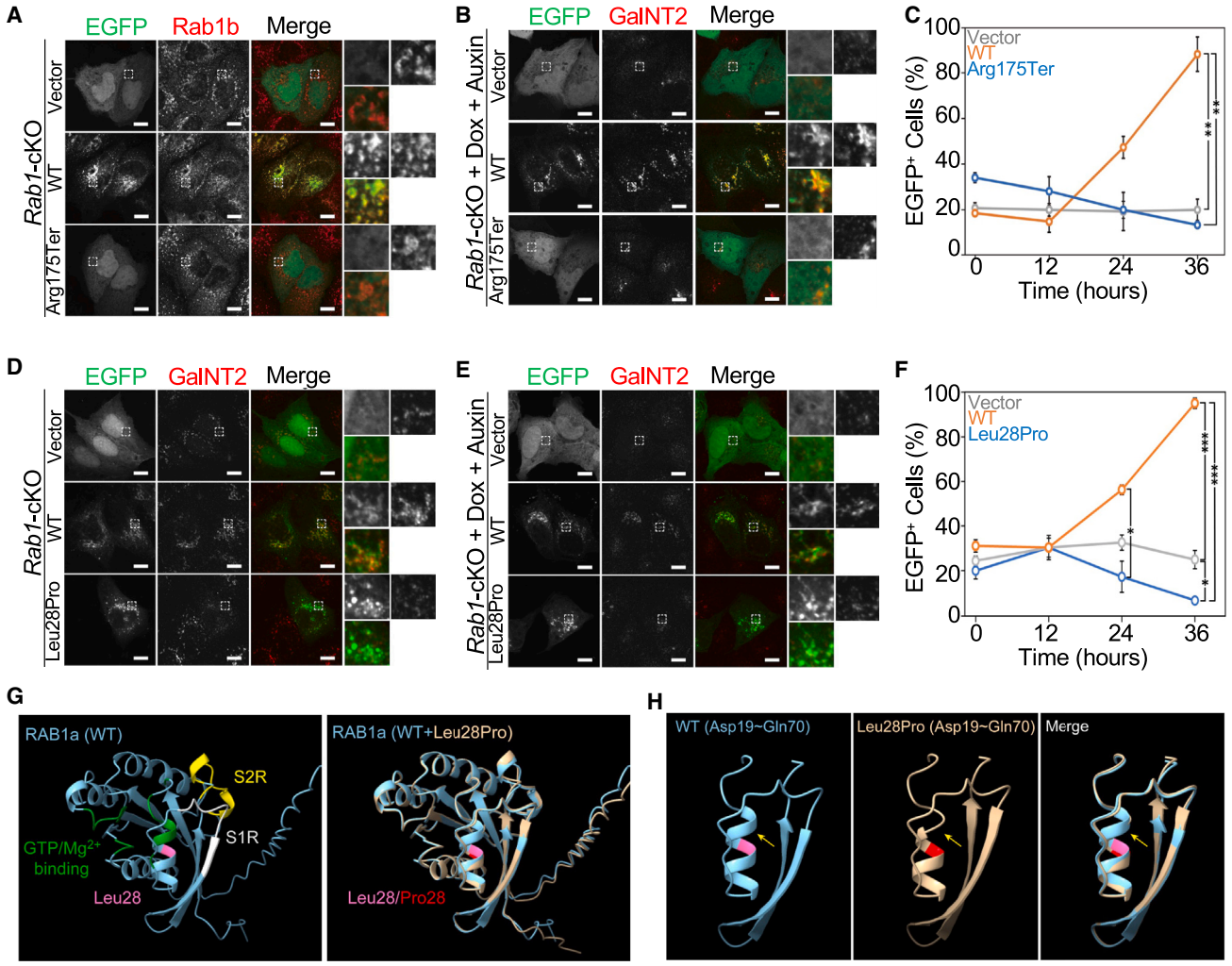

Figure 2. Variant RAB1a fail to rescue Golgi morphology in *Rab1*-depleted cells

(A and B) Co-localization of full-length (WT) and truncated (p.Arg175Ter) EGFP-RAB1a (green) with AID-tagged Rab1b or the *trans*-Golgi protein GalNT2 (red) in (A) untreated *Rab1*-cKO cells or (B) *Rab1*-depleted *Rab1*-cKO cells treated with doxycycline and auxin. Scale bar, 10 μm.

(C) Time-course quantification of EGFP^{+} *Rab1*-depleted *Rab1*-cKO cells treated with doxycycline and auxin expressing an empty vector (gray) construct or constructs encoding full-length (WT, orange) or truncated (p.Arg175Ter, blue) RAB1a. Mean and SEM are shown from three independent experiments. Statistically significant differences were determined by one-way ANOVA with Tukey's test. **$p < 0.01$.

(D and E) Co-localization of full-length (WT) and missense-variant (p.Leu28Pro) EGFP-RAB1a (green) with endogenous Golgi-localized GalNT2 (red) in (D) untreated *Rab1*-cKO cells or (E) *Rab1*-depleted *Rab1*-cKO cells treated with doxycycline and auxin. Scale bar, 10 μm.

(F) Time-course quantification of EGFP^{+} *Rab1*-depleted *Rab1*-cKO cells treated with doxycycline and auxin and expressing empty vector (gray) construct or constructs encoding full-length (WT, orange) or missense-variant (Leu28Pro, blue) RAB1a. Mean and SEM are shown from three independent experiments. Statistically significant differences were determined by one-way ANOVA with Tukey's test. *$p < 0.05$; ***$p < 0.001$.

(G) Predicted structures of wild-type and p.Leu28Pro RAB1a by AlphaFold2 using UniProt accession P62820.

(H) Predicted structure of wild-type and mutant switch 1 region (S1R) and GTP/Mg^{2+} binding site near the p.(Leu28Pro) variant of RAB1a.

RAB1a in *Rab1*-depleted cells rescued cell survival and proliferation compared to the empty vector negative control and compared to production of the truncated RAB1a (Figure 2C). Taken together, these results implicate RAB1a haploinsufficiency in the *RAB1A*-related neurocognitive disorder with speech and motor delay.

We then evaluated the potential for the missense-variant RAB1a (p.Leu28Pro) to rescue Golgi morphology and cell survival using *Rab1*-cKO cells. As expected in untreated *Rab1*-cKO cells, the full-length Rab1a co-localized with GalNT2 in the intact Golgi (Figure 2D). Surprisingly, production of the missense-variant RAB1a resulted in disruption of the Golgi compartment despite the cells retaining *Rab1b* expression, suggesting the missense mutation identified in the mosaic individual functions as a dominant negative (Figure 2D). Golgi morphology was rescued following production of the full-length, but not the missense-variant, RAB1a in treated *Rab1*-depleted cells (Figure 2E). Consistent with the LoF, or possibly dominant-negative function, of the missense-variant RAB1a,

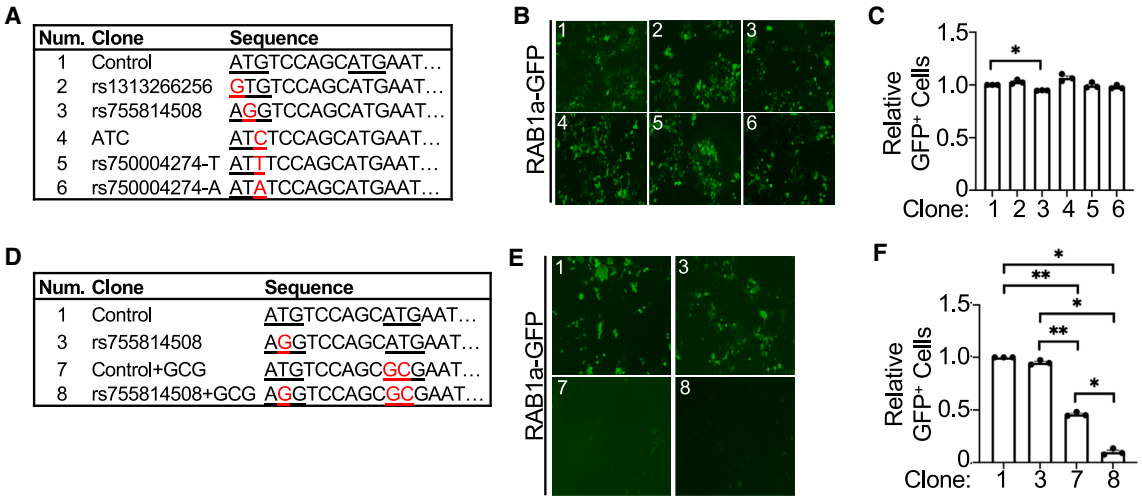

Figure 3. RAB1a is encoded by an alternative initiating methionine

(A) Schematic of initiating methionine variants tested following transient expression in HEK293 cells. Methionine-encoding codons are underlined. Engineered variants are shown in red.

(B) Representative images of HEK293 cells transiently expressing RAB1a-GFP clones shown in (A).

(C) Relative quantification of GFP$^+$ HEK293 cells expressing RAB1a-GFP clones from (A). Data represent mean and SEM relative to control from three independent experiments. Statistically significant differences compared to control were determined by one-way ANOVA with Dunnett test. *$p < 0.05$.

(D) Schematic of methionine-variant constructs tested for RAB1a-GFP production in HEK293 cells. Methionine-encoding codons are underlined. Engineered variants are shown in red.

(E) Representative images of HEK293 cells transiently expressing RAB1a-GFP constructs shown in (D).

(F) Relative quantification of GFP$^+$ HEK293 cells expressing RAB1a-GFP constructs from (D). Data represent mean and SEM relative to control from three independent experiments. Statistically significant differences were determined by one-way ANOVA with Tukey test. *$p < 0.05$; **$p < 0.01$.

production of the missense-variant RAB1a failed to rescue cell survival and proliferation in *Rab1*-depleted cells compared to the full-length RAB1a (Figure 2F). Using AlphaFold2 to model the structure of the missense-variant RAB1a, the p.Leu28Pro allele had little impact on the overall structure of RAB1a, though it was predicted to slightly alter the structure of the switch 1 region (S1R) and GTP/Mg^{2+} binding site of RAB1a (Figures 2G and 2H). Based on these results, the missense variant may alter GTP/GDP binding or GTPase activity of RAB1a.

The high LoF intolerance score and clinical association with haploinsufficiency among the individuals reported here suggest that LoF mutations would be rare in the general population. We identified multiple individuals in the BGL and gnomAD databases with variants predicted to disrupt the translation initiating methionine (p.Met1?) of the canonical transcript (GenBank: NM_004161.5), which would be considered potential LoF alleles. We hypothesized that these initiating methionine variants were not pathogenic and instead led to translation from an alternative in-frame methionine located 3 residues downstream. To test this, we cloned a region encoding an in-frame C-terminal GFP epitope immediately following the *RAB1A* coding sequence and transiently expressed in HEK293 cells the wild-type control transcript or transcripts containing different variants at the initiating methionine codon (Figure 3A). Because the C-terminal GFP epitope altered subcellular localization of RAB1a (data not shown), we quantified the relative number of RAB1a-GFP$^+$ cells by flow cytometry. In support of our hypothesis, all initiating methionine-variant constructs produced RAB1a-GFP at similar levels to control, with only a slight but statistically significant reduction for the rs755814508 allele (Figures 3B and 3C). These results suggest the encoded protein may initiate from the second in-frame methionine. To test this, we mutated the codons for p.Met1, p.Met4, or both and quantified RAB1a-GFP$^+$ cells by flow cytometry (Figure 3D). Mutation of the second methionine (Control+GCG) significantly reduced RAB1a-GFP production compared to control or to mutation of the first methionine (rs755814508) (Figures 3E and 3F). This was reduced further by altering both methionine residues (rs755814508+GCG) (Figures 3E and 3F). These results suggest the second in-frame methionine is the primary initiating residue in the canonical transcript and that the initiating methionine variants annotated in the gnomAD and BGL databases are likely benign polymorphisms. Of note, p.Met4? variants, which our results suggest would be LoF alleles, are not reported in the gnomAD or BGL databases.

Independent of its ER-Golgi trafficking functions, RAB1a was previously implicated in a "Golgi-bypass" transport pathway, localizing to the growth cones of developing neurites.[23] In addition to RAB1a, the Golgi-localized Atlastin 1 GTPase, encoded by *ATL1* (SPG3A [MIM: 606439]), also localizes to the growth cones of cultured neurons, as do REEP1 (SPG31 [MIM: 609139]) and Spastin (SPG4 [MIM: 604277]).[24,25] shRNA knockdown of *Atl1* in rat cortical

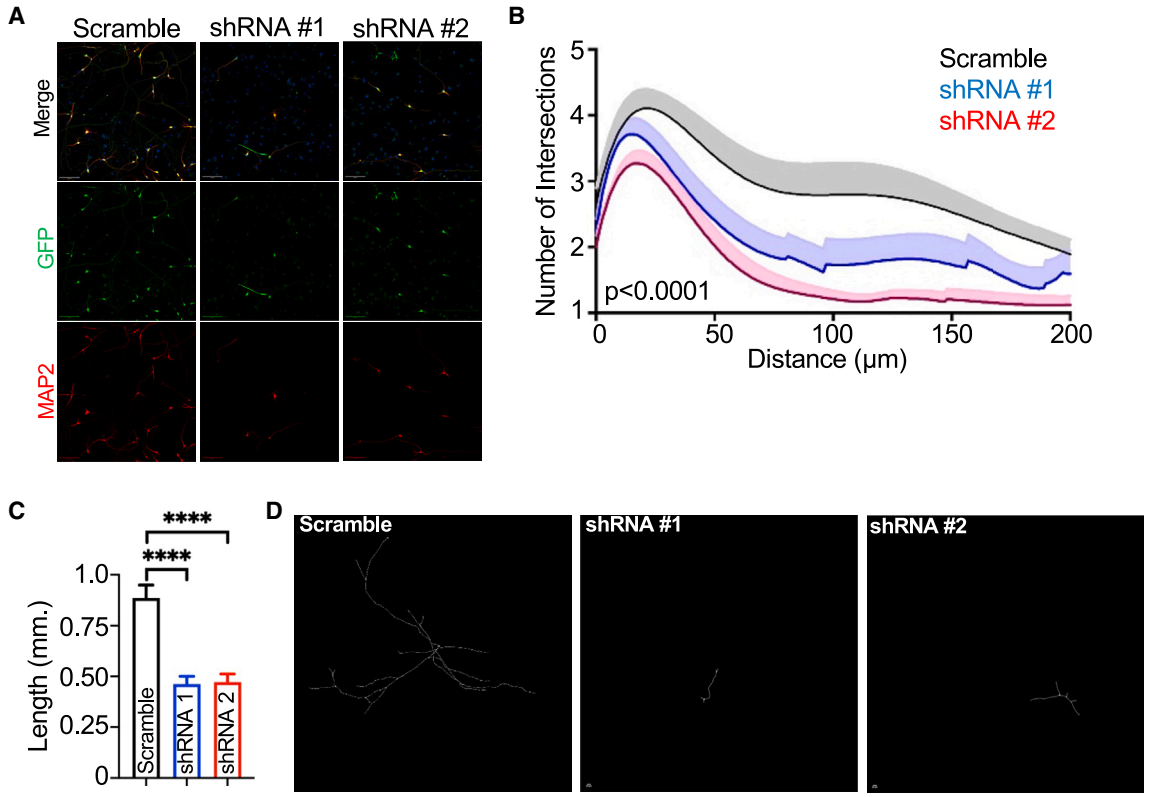

Figure 4. *RAB1A* is essential for dendritic morphogenesis

(A) Representative immunofluorescence images demonstrating the morphology of H9 human embryonic stem cell (hESC)-derived neurons following transfection with scramble shRNA control or two different shRNAs targeting *RAB1A*. Six days after transfection, neurons were stained with GFP to visualize and characterize neuronal morphology, MAP2 to indicate neuronal dendrites, and DAPI to mark nuclei. Scale bars, 100 μm.

(B) Sholl analysis shows a reduction in dendritic complexity in neurons transfected with two shRNAs targeting *RAB1A* (blue and red) compared to neurons transfected with scramble control shRNA (black). Data were analyzed using one-way ANOVA followed by Tukey's test. Mean and SEM are shown from n = 10 per group.

(C) Quantification of dendritic length in hESC-derived neurons following transfection with a scramble control shRNA (black) or shRNAs targeting *RAB1A* (blue and red). Data were analyzed using one-way ANOVA followed by Tukey's test. ****$p < 0.0001$. Mean and SEM are shown from n = 27 Scramble, n = 30 shRNA #1, and n = 32 shRNA #2.

(D) Representative tracings of hESC-derived neurons transfected with a scramble control shRNA or shRNAs targeting *RAB1A* utilized for Sholl analysis and dendritic length quantification. Scale bars, 20 μm.

neurons significantly reduced axon and dendrite growth, implicating impaired neuronal formation and/or differentiation in the pathogenesis of *ATL1*-associated HSP.[24] Therefore, we hypothesized that, like Atlastin 1, knockdown of the RAB1a GTPase impairs neuronal morphogenesis. To test this, we differentiated H9 human embryonic stem cells into neurons and transfected cells with a scramble shRNA (negative control) or two different shRNAs targeting *RAB1A*. Neurons transfected with the scramble control shRNA developed long, complex dendritic branches, while knockdown of *RAB1A* impaired dendritic arborization (Figure 4A). To quantify differences in dendritic complexity, we performed Sholl analysis of individual H9-derived neurons following transfection of scramble control shRNA or *RAB1A*-targeting shRNAs. Compared to scramble control, *RAB1A* knockdown significantly reduced dendritic length and complexity of neurons (Figures 4B–4D). These results demonstrate a critical role for *RAB1A* in neuronal morphogenesis, particularly in establishing dendritic length and arborization, and implicate impaired neuronal formation in the pathogenesis of the *RAB1A*-related neurocognitive disorder with speech and motor delay.

RAB1A is located on chromosome 2 within the 2p14–p15 microdeletion syndrome locus. Individuals with the 2p14–p15 microdeletion present with a variety of clinical sequelae, suggesting that individual genes within the microdeletion contribute to such clinical variability. For example, individuals whose microdeletion includes *OTX1* (MIM: 600036), encoding the orthodenticle homeobox 1, present with genitourinary defects.[26] Previously reported individuals harbor *de novo* 2p14–p15 microdeletions that include *RAB1A*[26–28]; therefore, we investigated similarities between their reported clinical manifestations (individuals 6–12) and those reported here with the *RAB1A*-related neurocognitive disorder with speech and motor delay (families 1–4) (Table 1). Almost all individuals from both diagnoses presented with speech and motor delay and variable neurocognitive involvement. Additionally, vision impairment,

microcephaly, and facial dysmorphisms were noted in both diagnoses, while skeletal and neuromuscular findings were variable. As well, additional individuals with similar clinical sequelae were identified in the DECIPHER genomics database with deletions overlapping *RAB1A*. Results from this study suggest that loss of *RAB1A* contributes to much of the neurodevelopmental manifestations of the 2p14–p15 microdeletion syndrome, including motor and neurocognitive deficiencies.

The RAB1a GTPase is highly conserved and is required for survival in multiple diverse species, including *Drosophila*,[29] yeast,[30] and nematode.[31] RAB1a regulates multiple fundamental cellular processes, such as ER-to-Golgi trafficking and autophagy, and also was implicated in the pathogenesis of Parkinson disease.[19,32–34] Here, we describe a *RAB1A*-related neurocognitive disorder with speech and motor delay caused by haploinsufficiency of *RAB1A*. We also propose that *RAB1A* haploinsufficiency is responsible for the neurodevelopmental manifestations of the 2p14–p15 microdeletion syndrome.

Data and code availability

The exome sequencing data are not publicly available due to privacy restrictions.

Supplemental information

Supplemental information can be found online at https://doi.org/10.1016/j.ajhg.2023.10.009.

Acknowledgments

The authors are thankful for the efforts of current and former laboratory members. Technical assistance was provided by the McDermott Center Next-Generation Sequencing Core and the McDermott Center Human Gene Discovery Laboratory at the University of Texas Southwestern Medical Center. Funding was provided by the Scottish Rite for Children research fund and the Spastic Paraplegia Foundation (both to J.J.R.). This work was also supported by Grant-in-Aid for Scientific Research (B) 22H02613 from the Ministry of Education, Culture, Sports, Science and Technology (MEXT) of Japan and by the Japan Science and Technology Agency (JST) CREST Grant JPMJCR17H4 (both to M.F.). Additional support was provided by the National Institutes of Health (R01HD099162 to M.H.C. and F31HD110206 to S.V.).

Declaration of interests

J.A.R., P.L., and W.B.: The Department of Molecular and Human Genetics at Baylor College of Medicine receives revenue from clinical genetic testing completed at Baylor Genetics Laboratory.

P.L. and W.B.: Baylor College of Medicine (BCM) and Miraca Holdings Inc. have formed a joint venture with shared ownership and governance of Baylor Genetics, which performs genetic testing and derives revenue. P.L. and W.B. are employees of BCM and derive support through a professional services agreement with Baylor Genetics.

Received: August 3, 2023
Accepted: October 10, 2023
Published: November 3, 2023

Web resources

AlphaFold2, https://alphafold.ebi.ac.uk
ChimeraX, https://www.rbvi.ucsf.edu/chimerax/
DECIPHER, https://www.deciphergenomics.org
GenBank, https://www.ncbi.nlm.nih.gov/genbank/
gnomAD, https://gnomad.broadinstitute.org
OMIM, https://www.omim.org
Partek, https://www.partek.com
Picard, http://broadinstitute.github.io/picard/
pVAAST, https://hufflab.org/software/pvaast/
SeattleSeq, https://snp.gs.washington.edu/SeattleSeqAnnotation154/

References

1. Fink, J.K. (2014). Hereditary spastic paraplegia: clinical principles and genetic advances. Semin. Neurol. *34*, 293–305. https://doi.org/10.1055/s-0034-1386767.
2. Blackstone, C. (2012). Cellular pathways of hereditary spastic paraplegia. Annu. Rev. Neurosci. *35*, 25–47. https://doi.org/10.1146/annurev-neuro-062111-150400.
3. Blackstone, C., O'Kane, C.J., and Reid, E. (2011). Hereditary spastic paraplegias: membrane traffic and the motor pathway. Nat. Rev. Neurosci. *12*, 31–42. https://doi.org/10.1038/nrn2946.
4. Esteves, T., Durr, A., Mundwiller, E., Loureiro, J.L., Boutry, M., Gonzalez, M.A., Gauthier, J., El-Hachimi, K.H., Depienne, C., Muriel, M.P., et al. (2014). Loss of association of REEP2 with membranes leads to hereditary spastic paraplegia. Am. J. Hum. Genet. *94*, 268–277. https://doi.org/10.1016/j.ajhg.2013.12.005.
5. Khan, T.N., Klar, J., Tariq, M., Anjum Baig, S., Malik, N.A., Yousaf, R., Baig, S.M., and Dahl, N. (2014). Evidence for autosomal recessive inheritance in SPG3A caused by homozygosity for a novel ATL1 missense mutation. Eur. J. Hum. Genet. *22*, 1180–1184. https://doi.org/10.1038/ejhg.2014.5.
6. D'Amico, A., Tessa, A., Sabino, A., Bertini, E., Santorelli, F.M., and Servidei, S. (2004). Incomplete penetrance in an SPG3A-linked family with a new mutation in the atlastin gene. Neurology *62*, 2138–2139.
7. Lindsey, J.C., Lusher, M.E., McDermott, C.J., White, K.D., Reid, E., Rubinsztein, D.C., Bashir, R., Hazan, J., Shaw, P.J., and Bushby, K.M. (2000). Mutation analysis of the spastin gene (SPG4) in patients with hereditary spastic paraparesis. J. Med. Genet. *37*, 759–765.
8. Sánchez-Ferrero, E., Coto, E., Beetz, C., Gámez, J., Corao, A.I., Díaz, M., Esteban, J., del Castillo, E., Moris, G., Infante, J., et al. (2013). SPG7 mutational screening in spastic paraplegia patients supports a dominant effect for some mutations and a pathogenic role for p.A510V. Clin. Genet. *83*, 257–262. https://doi.org/10.1111/j.1399-0004.2012.01896.x.
9. McDermott, C.J., Dayaratne, R.K., Tomkins, J., Lusher, M.E., Lindsey, J.C., Johnson, M.A., Casari, G., Turnbull, D.M., Bushby, K., and Shaw, P.J. (2001). Paraplegin gene analysis in hereditary spastic paraparesis (HSP) pedigrees in northeast England. Neurology *56*, 467–471.
10. Svenson, I.K., Kloos, M.T., Gaskell, P.C., Nance, M.A., Garbern, J.Y., Hisanaga, S.i., Pericak-Vance, M.A., Ashley-Koch, A.E.,

and Marchuk, D.A. (2004). Intragenic modifiers of hereditary spastic paraplegia due to spastin gene mutations. Neurogenetics *5*, 157–164. https://doi.org/10.1007/s10048-004-0186-z.

11. Depienne, C., Stevanin, G., Brice, A., and Durr, A. (2007). Hereditary spastic paraplegias: an update. Curr. Opin. Neurol. *20*, 674–680. https://doi.org/10.1097/WCO.0b013e3282f190ba.
12. Ngo, K.J., Rexach, J.E., Lee, H., Petty, L.E., Perlman, S., Valera, J.M., Deignan, J.L., Mao, Y., Aker, M., Posey, J.E., et al. (2020). A diagnostic ceiling for exome sequencing in cerebellar ataxia and related neurological disorders. Hum. Mutat. *41*, 487–501. https://doi.org/10.1002/humu.23946.
13. van de Warrenburg, B.P., Schouten, M.I., de Bot, S.T., Vermeer, S., Meijer, R., Pennings, M., Gilissen, C., Willemsen, M.A., Scheffer, H., and Kamsteeg, E.J. (2017). Clinical exome sequencing for cerebellar ataxia and spastic paraplegia uncovers novel gene-disease associations and unanticipated rare disorders. Eur. J. Hum. Genet. *25*, 393. https://doi.org/10.1038/ejhg.2016.168.
14. Yang, Y., Muzny, D.M., Xia, F., Niu, Z., Person, R., Ding, Y., Ward, P., Braxton, A., Wang, M., Buhay, C., et al. (2014). Molecular findings among patients referred for clinical whole-exome sequencing. JAMA *312*, 1870–1879. https://doi.org/10.1001/jama.2014.14601.
15. Hu, H., Roach, J.C., Coon, H., Guthery, S.L., Voelkerding, K.V., Margraf, R.L., Durtschi, J.D., Tavtigian, S.V., Shankaracharya, W., Wu, W., et al. (2014). A unified test of linkage analysis and rare-variant association for analysis of pedigree sequence data. Nat. Biotechnol. *32*, 663–669. https://doi.org/10.1038/nbt.2895.
16. Lek, M., Karczewski, K.J., Minikel, E.V., Samocha, K.E., Banks, E., Fennell, T., O'Donnell-Luria, A.H., Ware, J.S., Hill, A.J., Cummings, B.B., et al. (2016). Analysis of protein-coding genetic variation in 60,706 humans. Nature *536*, 285–291. https://doi.org/10.1038/nature19057.
17. Zheng, G.X.Y., Terry, J.M., Belgrader, P., Ryvkin, P., Bent, Z.W., Wilson, R., Ziraldo, S.B., Wheeler, T.D., McDermott, G.P., Zhu, J., et al. (2017). Massively parallel digital transcriptional profiling of single cells. Nat. Commun. *8*, 14049. https://doi.org/10.1038/ncomms14049.
18. Gomes, A.Q., Ali, B.R., Ramalho, J.S., Godfrey, R.F., Barral, D.C., Hume, A.N., and Seabra, M.C. (2003). Membrane targeting of Rab GTPases is influenced by the prenylation motif. Mol. Biol. Cell *14*, 1882–1899. https://doi.org/10.1091/mbc.e02-10-0639.
19. Stenmark, H. (2009). Rab GTPases as coordinators of vesicle traffic. Nat. Rev. Mol. Cell Biol. *10*, 513–525. https://doi.org/10.1038/nrm2728.
20. Farnsworth, C.C., Seabra, M.C., Ericsson, L.H., Gelb, M.H., and Glomset, J.A. (1994). Rab geranylgeranyl transferase catalyzes the geranylgeranylation of adjacent cysteines in the small GTPases Rab1A, Rab3A, and Rab5A. Proc. Natl. Acad. Sci. USA *91*, 11963–11967.
21. Hatoyama, Y., Homma, Y., Hiragi, S., and Fukuda, M. (2021). Establishment and analysis of conditional Rab1- and Rab5-knockout cells using the auxin-inducible degron system. J. Cell Sci. *134*, jcs259184. https://doi.org/10.1242/jcs.259184.
22. Homma, Y., Kinoshita, R., Kuchitsu, Y., Wawro, P.S., Marubashi, S., Oguchi, M.E., Ishida, M., Fujita, N., and Fukuda, M. (2019). Comprehensive knockout analysis of the Rab family GTPases in epithelial cells. J. Cell Biol. *218*, 2035–2050. https://doi.org/10.1083/jcb.201810134.
23. Sannerud, R., Marie, M., Nizak, C., Dale, H.A., Pernet-Gallay, K., Perez, F., Goud, B., and Saraste, J. (2006). Rab1 defines a novel pathway connecting the pre-Golgi intermediate compartment with the cell periphery. Mol. Biol. Cell *17*, 1514–1526. https://doi.org/10.1091/mbc.e05-08-0792.
24. Zhu, P.P., Soderblom, C., Tao-Cheng, J.H., Stadler, J., and Blackstone, C. (2006). SPG3A protein atlastin-1 is enriched in growth cones and promotes axon elongation during neuronal development. Hum. Mol. Genet. *15*, 1343–1353. https://doi.org/10.1093/hmg/ddl054.
25. Park, S.H., Zhu, P.P., Parker, R.L., and Blackstone, C. (2010). Hereditary spastic paraplegia proteins REEP1, spastin, and atlastin-1 coordinate microtubule interactions with the tubular ER network. J. Clin. Invest. *120*, 1097–1110. https://doi.org/10.1172/JCI40979.
26. Jorgez, C.J., Rosenfeld, J.A., Wilken, N.R., Vangapandu, H.V., Sahin, A., Pham, D., Carvalho, C.M.B., Bandholz, A., Miller, A., Weaver, D.D., et al. (2014). Genitourinary defects associated with genomic deletions in 2p15 encompassing OTX1. PLoS One *9*, e107028. https://doi.org/10.1371/journal.pone.0107028.
27. Hancarova, M., Vejvalkova, S., Trkova, M., Drabova, J., Dleskova, A., Vlckova, M., and Sedlacek, Z. (2013). Identification of a patient with intellectual disability and de novo 3.7 Mb deletion supports the existence of a novel microdeletion syndrome in 2p14-p15. Gene *516*, 158–161. https://doi.org/10.1016/j.gene.2012.12.027.
28. Wohlleber, E., Kirchhoff, M., Zink, A.M., Kreiss-Nachtsheim, M., Küchler, A., Jepsen, B., Kjaergaard, S., and Engels, H. (2011). Clinical and molecular characterization of two patients with overlapping de novo microdeletions in 2p14-p15 and mild mental retardation. Eur. J. Med. Genet. *54*, 67–72. https://doi.org/10.1016/j.ejmg.2010.09.012.
29. Chan, C.C., Scoggin, S., Wang, D., Cherry, S., Dembo, T., Greenberg, B., Jin, E.J., Kuey, C., Lopez, A., Mehta, S.Q., et al. (2011). Systematic discovery of Rab GTPases with synaptic functions in Drosophila. Curr. Biol. *21*, 1704–1715. https://doi.org/10.1016/j.cub.2011.08.058.
30. Segev, N., and Botstein, D. (1987). The ras-like yeast YPT1 gene is itself essential for growth, sporulation, and starvation response. Mol. Cell Biol. *7*, 2367–2377.
31. C elegans Deletion Mutant Consortium (2012). Large-scale screening for targeted knockouts in the Caenorhabditis elegans genome. G3 (Bethesda) *2*, 1415–1425. https://doi.org/10.1534/g3.112.003830.
32. Lynch-Day, M.A., Bhandari, D., Menon, S., Huang, J., Cai, H., Bartholomew, C.R., Brumell, J.H., Ferro-Novick, S., and Klionsky, D.J. (2010). Trs85 directs a Ypt1 GEF, TRAPPIII, to the phagophore to promote autophagy. Proc. Natl. Acad. Sci. USA *107*, 7811–7816. https://doi.org/10.1073/pnas.1000063107.
33. Wang, J., Menon, S., Yamasaki, A., Chou, H.T., Walz, T., Jiang, Y., and Ferro-Novick, S. (2013). Ypt1 recruits the Atg1 kinase to the preautophagosomal structure. Proc. Natl. Acad. Sci. USA *110*, 9800–9805. https://doi.org/10.1073/pnas.1302337110.
34. Cooper, A.A., Gitler, A.D., Cashikar, A., Haynes, C.M., Hill, K.J., Bhullar, B., Liu, K., Xu, K., Strathearn, K.E., Liu, F., et al. (2006). Alpha-synuclein blocks ER-Golgi traffic and Rab1 rescues neuron loss in Parkinson's models. Science *313*, 324–328. https://doi.org/10.1126/science.1129462.